Vaccine 41 (2023) 304–314

Contents lists available at ScienceDirect

Vaccine

journal homepage: www.elsevier.com/locate/vaccine

Intradermal delivery of a quadrivalent cell-based seasonal influenza vaccine using an adjuvanted skin patch vaccination platform

Thomas J. Ellison *, George C. Talbott, Daniel R. Henderson

Verndari Inc., 2700 Stockton Blvd., Suite 1104, Sacramento, CA 95817, United States

ARTICLE INFO

Article history:
Received 8 June 2022
Received in revised form 26 September 2022
Accepted 5 October 2022
Available online 13 December 2022

Keywords:
Flucelvax
VaxiPatch
Influenza vaccine
Cell-based vaccine
QS-21
3D-PHAD
Adjuvants
Microneedle
Skin patch
Microneedle array
Intradermal
VAS1.2
Needle-free

ABSTRACT

All seasonal influenza vaccines for 2021–2022 in the US were quadrivalent and the market continues to be dominated by intramuscular delivery of non-adjuvanted, virion-derived antigens grown in chicken eggs. Up to four new egg-adapted production influenza vaccine strains must be generated each year. The introduction in 2012 of Flucelvax®, which is grown in mammalian suspension cell culture and uses vaccine production strains without adaptive mutations for efficient growth in eggs, represented a major advance in vaccine production technology. Here we demonstrate that Flucelvax can be reformulated and combined with a liposomal adjuvant containing QS-21 (Verndari Adjuvant System 1.1, VAS1.1) or QS-21 and 3D-PHAD (VAS1.2) for intradermal administration using a painless skin patch, VaxiPatch™. VAS1.2 is similar to $AS01_B$, the adjuvant system used in Shingrix® and Mosquirix™. We show that Flucelvax, when reformulated and concentrated using tangential flow filtration (TFF), maintains hemagglutination and single radial immunodiffusion (SRID) potency. Loading the reformulated Flucelvax material onto VaxiPatch arrays conferred high levels of resistance to heat stress and room temperature stability. TFF enriched vaccine antigens were combined with VAS1.1 or VAS1.2 and dispensed in 10nL drops into the pockets of 36 (total 360 nL) stainless steel microneedles arranged in a microarray 1.2 cm in diameter. Using VaxiPatch delivery of 2 μg of antigen, we demonstrated intramusuclar-comparable IgG and hemagglutination inhibition (HAI) immune responses in Sprague Dawley® rats. With addition of VAS1.2, antigen-specific IgG titers were increased as much as 68-fold (47-fold for VAS1.1) with improvements in seroconversion for three of four strains (all four were improved by VAS1.1). TFF-reformulated antigens combined with VAS1.1 or VAS1.2 and delivered by VaxiPatch showed only minor skin reactogenicity after 1 h and no skin reactogenicity after 24 h. These data indicate that VaxiPatch and the VAS system have the potential to be transformative for vaccine delivery.

1. Introduction

Current seasonal influenza vaccines are developed based on four influenza virus strains (quadrivalent, QIV) chosen a year in advance by the World Health Organization (WHO). Each year, new vaccine production strains are generated, tested, selected for suitability, and mass-produced in eggs or tissue culture. The development, manufacturing, and FDA approval process from choosing the vaccine strains to distributing product consumes roughly 7–9 months [1–3]. The interim US Flu vaccine effectiveness (VE) data for 2021–2022 calculated by the CDC indicated an overall VE of 16 % [4]. In the elderly 65+ age group, the interim VE was 9 %. Final 2021–2022 VE data will be available later this year, but it is clear that seasonal influenza vaccines need significant improvement.

In contrast, the COVID-19 mRNA vaccines from Pfizer/BioNTech and Moderna demonstrated VEs ~95 % after two doses [5,6]. RNA-based vaccines may enable rapid product modifications to address strain changes [7,8]. Consequently, more than ten mRNA influenza vaccines are known to be currently in development [9]. However, mRNA vaccines developed against COVID-19 have more adverse events compared to marketed influenza vaccines [10,11], they need to be frozen throughout storage and distribution [12], and they do not give durable protection from disease [13].

A second approach to improve seasonal influenza vaccines is through adjuvants to enhance the magnitude, durability and/or type of immune response. Only one FDA approved seasonal influenza vaccine uses an adjuvant; Fluad® is an egg-based QIV vaccine using the oil emulsion adjuvant MF59 [14]. Fluad has shown increased cross-clade protection; this characteristic could

* Corresponding author.
E-mail addresses: tellison@verndariinc.com (T.J. Ellison), gtalbott@verndariinc.com (G.C. Talbott), dhenderson@verndariinc.com (D.R. Henderson).

https://doi.org/10.1016/j.vaccine.2022.10.006
0264-410X/

ultimately enable a universal flu vaccine [15]. However, Fluad requires refrigeration and is given by traditional intramuscular (IM) injection.

Prior to the success of mRNA vaccines, great strides were made in intradermal vaccination research, including reduction of vaccine dose required [16], elimination of hypodermic needles, and thermostability. These innovative approaches promised the possibility of self-administration, durable protective responses, distribution through the mail, and increasing global vaccine availability. Simplified administration and distribution have the potential to accelerate the global response to pandemics threatened by agents such as influenza, Ebola, and COVID-19 [17].

We developed a microneedle array skin patch (VaxiPatch™) to enable vaccines that are room temperature-stable, painless, and could potentially be self-applied. Our initial proof-of-concept for VaxiPatch combined a recombinant monovalent influenza antigen with a dried version of the saponin adjuvant QS-21, with or without the Toll-Like Receptor 4 (TLR4) agonist 3D-PHAD [18].

In the work described here we further develop VAS1.1, a liposomal saponin adjuvant, and VAS1.2, an adjuvant which is analogous to $AS01_B$, a constituent in both the malaria vaccine Mosquirix™ and the shingles vaccine Shingrix®. $AS01_B$ is efficient at promoting $CD4^+$ T cell-mediated immune responses, an attractive attribute for vaccines targeting viruses or intracellular pathogens [19–21]. With the incorporation of $AS01_B$, the protein subunit vaccine Shingrix has a VE of 97 % and provides durable life-long immunity [22]. Here we have combined VAS1.1 or VAS1.2 with the cell-based QIV vaccine Flucelvax and delivered the vaccine and adjuvant combination on VaxiPatch in Sprague Dawley rats.

We demonstrate a three-pronged technology using: (1) approximately 0.5 μg of each hemagglutinin (HA) from the QIV 2019–2020 Flucelvax seasonal influenza vaccine, (2) 0.5 μg of the adjuvant QS-21 alone (as VAS1.1) or in combination with 0.5 μg of the adjuvant 3D-PHAD (as VAS1.2) and (3) VaxiPatch, a novel microneedle platform. Vaccinating rats with this configuration yielded midpoint IgG titers 8–68 times higher, with better seroconversion rates than IM Flucelvax.

2. Materials and methods

2.1. Sourcing of vaccine material

The 2019–2020 Northern Hemisphere (NH) formulation of Flucelvax Quadrivalent was obtained from Seqirus (Lot 261198, exp. June 2020). Shingrix (GSK) was purchased on the open market.

2.2. Tangential flow filtration (TFF)

Hollow fiber filters with 500kD molecular weight cut-off (MWCO) membranes (Spectrum Labs C02-E500-05-N, 20 cm^2 0.5 mm ID) were washed with Water for Injection (WFI, Cytiva SH30221.10), sanitized with 20 % USP ethanol (Spectrum Chemical ET107), and equilibrated into formulation buffer (10 mM NaP, 140 mM NaCl, 15 % w/v trehalose; pH 7.20). A syringe adapter kit (Spectrum Labs ACPX-400–01 N) was used with 50 mL syringes (Becton Dickinson 309653) to cycle the TFF unit manually. Retentate was 0.2μ-filtered (Cytiva 6780–2502) and concentrated on a 100 k_D diafiltration spin column (EMD Millipore UFC510024). Protein levels were assessed by Bicinchoninic Acid (BCA) assay (Thermo Scientific 23227).

2.3. Hemagglutination assay

Single-donor O+ human erythrocytes (hRBCs, Innovative Research) were washed and calibrated to a 0.75 % packed cell volume suspension (~$6x10^7$ cells/mL). Samples were serially diluted in phosphate-buffered saline (PBS, Cytiva SH30028.03) in U-bottom assay plates (Costar 3363) followed by addition of 50 μL of the hRBC suspension. Plates were incubated at room temperature (RT) for 60 min. Agglutination titers were defined as the last dilution which prevented "halo-like" settling of the hRBCs.

2.4. Liposomal adjuvant preparation

Structural lipid components were prepared as stocks in chloroform (Acros Organics 390760010): 1,2-dioleoyl-*sn-glycero*-3-phosphocholine (DOPC) (Avanti Polar Lipids 850375C) and plant cholesterol (Avanti Polar Lipids 700100P) were mixed at a mass ratio of 4:1 (DOPC:chol) in glass test tubes, then dried to a thin film under a stream of argon gas. 3D(6-acyl) PHAD® (3D-PHAD) (Avanti 699855) was included in films destined for VAS1.2 (mass ratio of 4:1:1 DOPC:Chol:3D-PHAD). Films were hydrated at 20 mg/mL total lipid in formulation buffer (10 mM NaP, 140 mM NaCl, 15 % w/v trehalose, pH 7.20) for 30 min with mixing to form initially heterogeneous structures. Lipid hydrate was loaded into an Extrusion Kit (Avanti 610000) with a 0.1μ polycarbonate membrane, passed through the membrane 21 times, and recovered into the permeation syringe as highly ordered liposomes. For 3D-PHAD liposomes, extrusion was performed at 37 °C, resulting in 3D-PHAD incorporation into the lipid bilayer. Concentration of the structural lipids and 3D-PHAD were determined by high performance liquid chromatography with an evaporative light-scattering detector (HPLC-ELSD).

QS-21 (Croda Health) stocks were prepared at 2.5 mg/mL in resuspension buffer (10 mM NaP; pH 6.40), diluted 1:1 in loading buffer (10 mM NaP, 280 mM NaCl, 30 % trehalose; pH 7.20), and mixed with extruded liposomes for 30 min at RT to allow binding of QS-21 to cholesterol on the outer leaflet of the liposomes. A spin diafiltration unit with a 100 k_D MWCO membrane (Amicon Ultra-0.5 100 K, EMD Millipore UFC510024) was used to concentrate the QS-21-loaded liposomes at 4000 g and 10 °C. HPLC-ELSD was used to measure final concentration of both adjuvant components.

2.5. Nanoparticle analysis

Samples for Dynamic Light Scattering (DLS) were diluted, and three to six measurements were collected per sample using a Malvern Nano ZS. Surface charge (Zeta potential) samples were diluted in water and loaded into disposable capillary cells (Malvern DTS1070).

2.6. Hemolysis quenching assay

hRBCs were washed with PBS and adjusted to 2×10^8 cells/mL. Hemolytic activity of QS-21 was assessed by 2-fold dilutions of samples in PBS in a U-bottom 96-well plate (Costar 3363), followed by addition of $1x10^7$ hRBCs/well and incubation for 30 min at RT. Plates were centrifuged at 900*g* for 6 min to sediment intact RBCs. Supernatants were transferred to flat-bottom 96-well assay plates (Costar 3370) and absorbance was measured at 450 nm (AccuSkan FC plate reader, Fisher Scientific). For quenching experiments, serial dilutions of DOPC/cholesterol liposomes in PBS were prepared, and a fixed dose of QS-21 (1μg per well) was added. After 15 min, hRBCs were added and incubated, followed by centrifugation and assessment of absorbance in the supernatant as above.

2.7. CryoEM imaging of liposomal adjuvants

Samples were imaged by CryoEM at the Biological EM Core Facility at UC Davis. Briefly, samples were applied to a glow discharged Quantifoil R1.2/1.3 300 mesh transmission electron micro-

scopy (TEM) grid. Automatic blotting and plunge freezing were performed using a Leica EM GP2 plunger. Grids were loaded into a Thermo Fisher Glacios operated at 200 kV and imaged with a low dose condition (50 e/Å^2) using a Gatan K3 direct electron detector. Images were collected at 45,000x nominal magnification with an 0.88 Å/pix calibrated pixel size using SerialEM.

2.8. Quantitative analysis of adjuvants by HPLC-ELSD

HPLC analysis was performed on a Shimadzu Nexera-i LC-2040C with an evaporative light-scattering detector (ELSD-LTIII, Shimadzu) fitted with a Restek Roc C18 5-μm reverse-phase (RP) column (150 mm × 4.6 mm). Solvents used were a) HPLC-grade H_20 (Fisher Chemical W5-4), b) isopropanol (Fisher Chemical A464-4) plus 0.1 % trifluoroacetic acid (TFA, ProteoChem LC6203-10amps), and c) 95 % methanol (Fisher Chemical A452-4) / 5 % H_20 plus 0.1 % TFA. A flow rate of 1.5 mL/min with a column temperature of 45 °C was used. ELSD detection was performed under nitrogen gas at a drift tube temperature of 40 °C. Extraction of samples was performed by 5-fold dilution in chloroform followed by a 6.67-fold dilution in methanol to merge phases (40-fold cumulative dilution of initial sample). Limits of quantitation were calculated using single-component standard curve material.

2.9. Microarray Loading, Imaging, and elution

VaxiPatch arrays were fabricated and loaded as described elsewhere [18]. In brief, antigen, with or without VAS adjuvant, was formulated with Ethylenediamine Tetraacetic Acid (EDTA, Fisher Chemical S312-500) to 1 mM, and Food, Drug, and Cosmetics (FD&C) Blue no. 1 dye (Spectrum Chemicals FD110) to 0.5 % (w/v) prior to microfluidic dispensing onto stainless-steel VaxiPatch arrays. Each microneedle tip was loaded with 10nL of the formulated concentrate, for a total of 0.36 μL per VaxiPatch microarray. Final trehalose mass ratios of VAS1.1 and VAS1.2 arrays were 10.5 and 20 g / g lipid, respectively. Imaging and assessment of delivery by residual dye elution was also performed as previously described [18].

2.10. Animal studies

All animal studies were approved by the UC Davis Institutional Animal Care and Use Committee (IACUC), Protocol No. 21302, and were performed by staff at the UC Davis Mouse Biology Program (MBP) as described previously [18]. For this study, groups of eight rats (4 of each gender) were utilized.

2.11. ELISA assays

IgG enzyme-linked immunosorbant assay (ELISA) assays for B/Colorado/06/2017 were performed as described elsewhere [18]. The recombinant hemagglutinins (HAs) representing the other three vaccine strains were purchased (IT-003-00110ΔTMp, IT-003-00436ΔTMp, IT-003-B11ΔTMp, Immune Technology). HAs in 100 mM sodium carbonate (Alfa Aesar, J62610) were used to coat H1N1 and H3N2 antigens. Monoclonal antibody positive controls for H1N1, B-Vic, and B-Yam assays were purchased (Immune Technology; IT-003–00105 M1, IT-003-B21M4, and IT-003-B11M6). For the H3N2 ELISAs, we used MIA-H3-HK214 (eEnzyme) as the positive control antibody. For midpoint titer analyses, a power trendline was plotted for each sample based on serum dilution factor and raw absorbance at 450 nm. This curve was used to calculate a theoretical dilution factor to achieve an absorbance of 0.5, to derive normally distributed data for statistical analysis.

2.12. Hemagglutination inhibition assays

For hemagglutination inhibition (HAI) assays, human erythrocytes were sourced and washed as above. 2019–2020 WHO antigens, BPL-Inactivated: A/Brisbane/02/2018 (FR-1730), A/Kansas/14/2017 (FR-1731), B/Colorado/06/2017 (FR-1607), and B/Phuket/3073/2013 (FR-1734) were obtained through the International Reagent Resource, Influenza Division, WHO Collaborating Center for Surveillance, Epidemiology and Control of Influenza, Centers for Disease Control and Prevention, Atlanta, GA, USA. These beta-propiolactone-inactivated (BPL) standards were used to prepare stocks at 8 hemagglutinating units (HAU) per 50 μL, which were confirmed by back titration. Kaolin treatment and hemagglutination inhibition assays of the rat serum were performed as previously described [18].

2.13. Vaccine material potency and stability studies

Vaccine potency was determined by single radial immunodiffusion (SRID) as described elsewhere [18]. Egg-based antigens and antisera for 2019–2020 strains were obtained from the National Institute for Biological Standards and Control (18/238 and 19/102 for A/Brisbane/02/2018, 19/104 and 19/152 for A/Kansas/14/2017, 18/104 and 18/170 for B/Colorado/06/2017, and 16/158 and 17/214 for B/Phuket/3073/2013. NIBSC, Potters Bar, UK).

For stability studies, vaccine material was printed at 4 μg/array, without adjuvant. Arrays were sealed in foil bags containing desiccant and stored at 20 °C overnight, then segregated to storage temperatures of 4, 20, 40, or 60 °C. At designated times, three arrays per timepoint were sequentially eluted into 115 μL of PBS, for Zwittergent treatment and SRID to determine HA potency. Stability control samples (liquid Flucelvax) were stored at 4° or 40 °C in sterile tubes for 28 days prior to evaluation by hemagglutination assay.

2.14. Statistical analysis

ELISA IgG midpoint titers and HAI titers at week 4 post-vaccination were log transformed prior to one-way ANOVA test followed by post-hoc Tukey's HSD tests (Microsoft Excel).

3. Results

3.1. Re-formulation of quadrivalent cell-based antigen preserves vaccine structure and activity

Flucelvax antigens were re-formulated by tangential flow filtration (TFF) into a buffered trehalose solution for loading onto VaxiPatch arrays. 25 doses of the 2019–2020 NH formulation of Flucelvax were diluted 2.14-fold in formulation buffer (phosphate-buffered saline with 15 % trehalose) and loaded onto hollow fiber filters. This material was processed down to minimal hold-up volume (~0.75 mL) twice, with one additional change of buffer (30 mL). To assess retention of the antigen across reformulation, hemagglutination assays using the input, retentate, and permeate material were performed (Fig. 1A). As shown in Fig. 1A, ~64 % of the total HA activity was retained through processing. Minimal loss of HA activity to membrane permeation was observed (<3%, Fig. 1B). The input material was heterogeneous by DLS (PdI = 0.527), whereas polydispersity decreased through tangential flow filtration and 0.2μ filtration (Fig. 1C and S1). Z-average size decreased through TFF processing, from an initial value of 93.72 nm in Flucelvax to 71.4 nm in the sterile filtrate. An additional 6.4-fold concentration was achieved by spin diafiltration (100kD MWCO) after sterile filtration of the TFF retentate. Protein

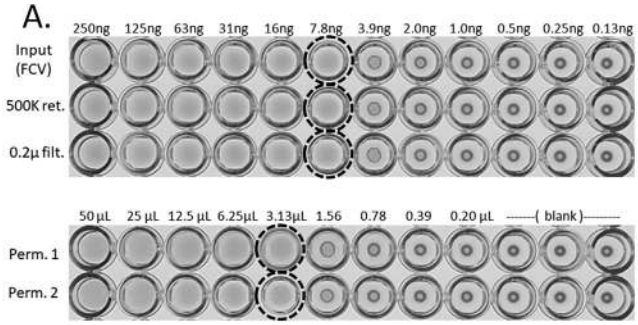

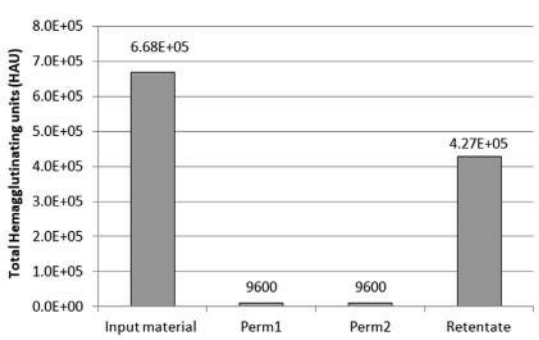

C.

	Z-average (nm)	σ Z-avg	PdI	σ PdI
Input (FCV)	93.72	4.74	0.527	0.03
TFF retentate	78.91	0.72	0.361	0.03
0.2µ filtered	71.40	2.28	0.287	0.03
concentrated	56.22	2.03	0.315	0.05

D.

HA strain for SRID test:	type:	Potent HA dose (ng)
A/Brisbane/02/2018	H1N1	554.07
A/Kansas/14/2017	H3N2	465.62
B/Colorado/06/2017	B-Vic	438.08
B/Phuket/3073/2013	B-Yam	602.82
Total potent HA:		2060.59
Percent total protein mass:		103%

Fig. 1. Reformulation of Flucelvax by TFF. A) Hemagglutination assay on 500 K 0.5 mm mPES TFF fractions of'19-'20 NH Flucelvax. Input and retentate loaded in a 2-fold dilution series from 250 ng (total protein by BCA assay). Permeate samples were loaded as serial dilutions by volume. Final dilution with full agglutination is indicated by yellow circles (lack of "halo" pattern of settled hRBCs). B) Comparison of total hemagglutinating units (HAU) by fraction. C) Summary table of DLS values for reformulated quadrivalent antigen. D) Potency by strain in concentrated/reformulated Flucelvax material based on analogous SRID reagents, per 0.36 µL (single array dose).

recovery for the final spin concentration step was >92 % by BCA assay. This concentrate was assessed for integrity by DLS, with results as summarized in Fig. 1C. The spin diafiltration step was associated with a further decrease in polydispersity, and a decrease in particle size, to 56.22 nm.

SRID was conducted on the concentrate to assess levels of potent HA by strain as described above (Fig. 1D). When calculated for the final 0.36 µL formulated VaxiPatch dose, single-strain equivalent doses of potent HA were between 438 ng (B-Victoria) and 602 ng (B-Yamagata), and the sum of potent HA mass agreed closely with total protein content by BCA assay.

3.2. Generation and characterization of liposomal adjuvant

Through use of an extrusion method, 3D-PHAD can be incorporated directly into the DOPC/cholesterol liposomes during formation. Extrusion remains efficient at high lipid concentrations (>20 mg/mL), and can be performed in the presence of trehalose, allowing direct generation of highly concentrated preparations. QS-21 is loaded in a finishing step.

To verify quenching of the hemolytic capacity of QS-21, we compared DOPC liposomes with different mass ratios (17 % and 28 % cholesterol by mass) for interference with hRBC lysis caused by 1 µg of QS-21, as shown in Fig. 2A. Above 1 µg of liposomes, hemolysis was quenched in both cases. We selected 18 % cholesterol as the mass ratio for use in both VAS1.1 and VAS1.2. We also verified that incorporation of 3D-PHAD into DOPC/cholesterol liposomes did not diminish their ability to quench QS-21 hemolysis (data not shown).

3D-PHAD was incorporated directly into highly homogeneous trehalose-containing liposomes with resulting diameters of 110–120 nm and PdI scores consistently less than 0.1 (Fig. 2B). For the VAS1.1 adjuvant, liposomes were extruded without 3D-PHAD. Diameters and PdI scores, as assessed by DLS, for these DOPC/cholesterol liposomes were comparable. Incorporation of the 3D-PHAD was associated with a notable shift in surface charge from near-neutral (−1.19 mV) to −42.43 mV (Fig. 2C).

QS-21 was loaded onto liposomes to form VAS1.1 or VAS1.2. The QS-21 loading ratio was guided by hemolysis quenching experiments, which suggested that QS-21 was efficiently quenched by a 2-fold excess of lipid. For VAS1.2, the loading ratio took into account the pre-determined 3D-PHAD content to match the doses of the two adjuvants. For both VAS1.1 and VAS1.2, loading with QS-21 was associated with slight decreases in Z-average and surface charge, but the adjuvant preparations remained unimodal with low polydispersity (<0.1 PdI) in all cases.

For comparison, a sample of the liposomal dual-adjuvant $AS01_B$ was obtained from the Shingrix vaccine (GSK). Shingrix ships in two vials, one containing the lyophilized antigen, and the other filled with an aqueous suspension of $AS01_B$. We subjected $AS01_B$ to DLS and zeta potential analysis. Empty liposomes, VAS1.2, and $AS01_B$ were also imaged by CryoEM, as shown in Fig. 2D. All showed a spherical shape with consistent unilamellar structure, with both VAS1.2 and $AS01_B$ presenting a mottled surface appearance as compared to the empty liposomes which lacked QS-21.

3.3. Quantitative analysis of VAS1.1 and VAS1.2

We developed an HPLC-ELSD method for quantifying all components of the VAS adjuvant system simultaneously, along with an extraction method to prepare aqueous samples for analysis. The time program for the solvent gradient is shown in Fig. 3A. Calibration curves for DOPC, cholesterol, QS-21, and 3D-PHAD were established, and lower limits of quantitation between 2.07 (cholesterol) and 5.65 (QS-21) ng/µL were calculated, as shown in Fig. 3B.

A chromatogram trace of a VAS1.2 preparation is shown in the upper panel of Fig. 3C, showing peaks associated with QS-21, DOPC, cholesterol, and 3D-PHAD, respectively. In the lower panel, a 10-fold concentrated sample of $AS01_B$ is shown, with identical retention times for QS-21, DOPC, and cholesterol components. The naturally derived MPLA component of $AS01_B$ eluted across a broad range, but also presented a small, discrete peak at a near-identical retention time as 3D-PHAD.

Concentrations of the four components from this analysis were normalized to 0.5 µg of QS-21 (our single-VaxiPatch dose) and used to generate the comparison table shown in Fig. 3D. For both VAS1.1 and VAS1.2, a consistent cholesterol mass percentage (18 %) was maintained. QS-21 loading was performed at roughly

A.

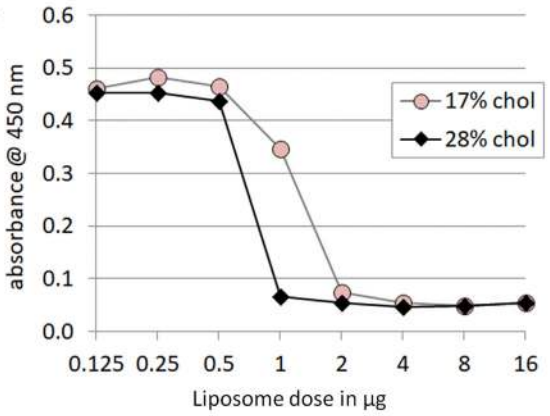

B.

	Z-Average (nm)	σ Z-avg	PdI	σ PdI
DOPC/chol liposomes	**119.2**	0.57	**0.083**	0.019
VAS1.1 (QS-21 loaded)	**117.6**	2.30	**0.095**	0.028
3D-PHAD liposomes	**112.6**	1.16	**0.073**	0.015
VAS1.2 (PHAD+QS-21)	**93.0**	0.69	**0.090**	0.015
$AS01_B$ (Shingrix®)	**99.8**	1.96	**0.145**	0.017

C.

	Zeta pot. (mV)	σ Zeta
DOPC/chol liposomes	**-1.19**	0.075
VAS1.1 (QS-21 loaded)	**-30.17**	1.002
3D-PHAD liposomes	**-42.43**	1.210
VAS1.2 (PHAD+QS-21)	**-48.20**	0.781
$AS01_B$ (Shingrix®)	**-29.47**	1.419

D.

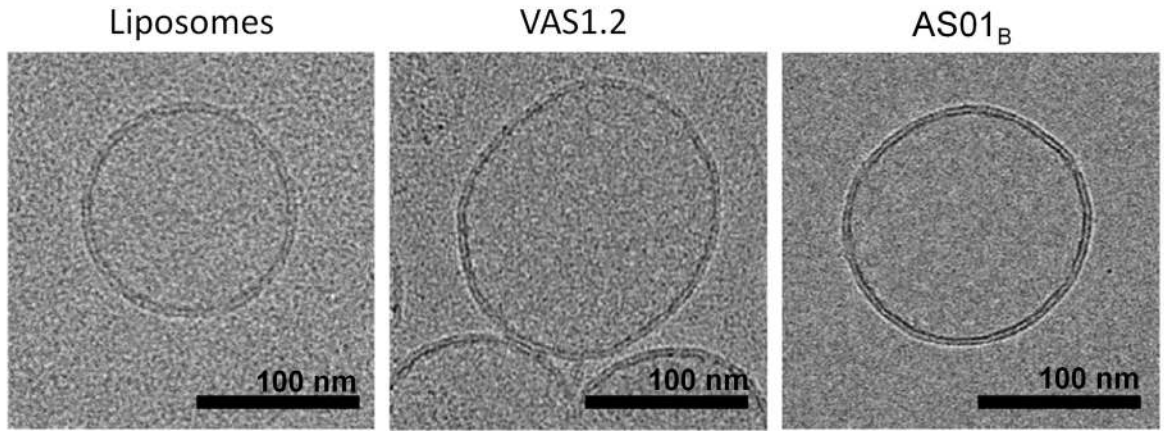

Fig. 2. Characterization of Liposomal Adjuvants. A) Quenching of hemolysis from 1 µg QS-21 by cholesterol/DOPC liposomes with varying cholesterol content by mass. B) Summary table of DLS data for liposomes and liposomal adjuvants, as compared to $AS01_B$. C) Zeta potential comparisons of VAS adjuvants and their liposomal precursors, as compared with $AS01_B$. D) CryoEM images of empty DOPC/chol liposomes (left panel) as compared to VAS1.2 (center) and $AS01_B$ adjuvant (right panel). Black scale bar shown in each image represents 100 nm.

twice the density per liposome for VAS1.2 in order to match the already-incorporated 3D-PHAD dose. This still represents a 4.3-fold excess of lipid for purposes of hemolysis quenching. By comparison, $AS01_B$ was considerably (7.67-fold) lower in relative QS-21 content as compared to total lipid in VAS1.2.

3.4. Animal studies for quadrivalent VaxiPatch

Four vaccine preparations were tested in Sprague-Dawley rats. Three groups received VaxiPatches (non-adjuvanted, +VAS1.1 at 0.5 µg QS-21, or +VAS1.2 at 0.5 µg QS-21 and 0.5 µg 3D-PHAD). The fourth group received an intramuscular injection of 50 µL of Flucelvax (1/10th of a normal human dose). Based on BCA assay, the IM injection animals received 18.5 µg of protein, as compared to the 2.0 µg of protein antigen loaded for each of the three intradermal VaxiPatch groups.

The top panel of Fig. 4A shows three detail images of tips loaded with VAS1.2 adjuvanted antigen, dried as a sugar glass. In the lower panel, tips were imaged on spent VaxiPatch arrays following 5-minute animal treatments. Delivery from all groups was high, with averages between 89 and 96 percent, as summarized in Fig. 4B. Images of four representative VAS1.1-adjuvanted array application sites are shown in Fig. 4C.

Finally, sites of array application were assessed using the zero-to-four Modified Draize Scale for redness (erythema) and swelling (oedema). Transient swelling was noted for 11 of 24 (45.8 %) of the animals, with a single animal (4.2 %) presenting moderate swelling (score of 2). In all animals, this swelling resolved after 1 h, and there was no increase in swelling among adjuvanted groups. The pre-vaccination hair removal protocol was associated with mild erythema in half of the animals (12 of 24), with scores of 1 recorded *prior* to VaxiPatch treatment (examples in Figure S2). None of these animals exhibited exacerbation of this pre-existing erythema post-treatment. Two animals developed transient mild erythema (scores of 1) at 1-hour post-treatment that resolved before the next timepoint at 24 h. One animal treated with a VAS1.1 array exhibited a delayed development of a mild erythema (score of 1) at 1 day post-treatment, which resolved prior to day 5. Full reactogenicity results are summarized in Figure S3. Cumulatively, release of vaccine material was efficient for all three VaxiPatch groups and was not associated with any significant or lingering reactogenicity.

3.5. Immunogenicity of VaxiPatch-delivered quadrivalent influenza vaccine

Antigen-specific serum IgG responses were assessed at day 28 post-vaccination. Coating antigens were selected as closest-equivalents to the cell-based vaccine strains included in Flucelvax. Pre-immune sera for all 32 animals were screened against all four strains, and all lacked sufficient reactivity to assign midpoint titers (data not shown). Fig. 5 compares day 28 IgG responses based on calculated midpoint titers for better representation of the natural variation between animals. For all four strains, differences in responses between the 18.5 µg IM injection dose and the 2.0 µg non-adjuvanted VaxiPatch dose were statistically insignificant,

A.

minutes	A: H20	B: IPA+TFA	C: 95% MeOH+TFA
0	26.3%	0%	73.7%
1	26.3%	0%	73.7%
5	0%	0%	100%
6	0%	55%	45%
10	0%	55%	45%
10.01	0%	100%	0%
17.5	0%	100%	0%
17.51	26.3%	0%	73.7%
20	26.3%	0%	73.7%

B.

Limit of Quantitation (ng/μL)	
DOPC	2.21
Cholesterol	2.07
QS-21	5.65
3D-PHAD	5.10

C.

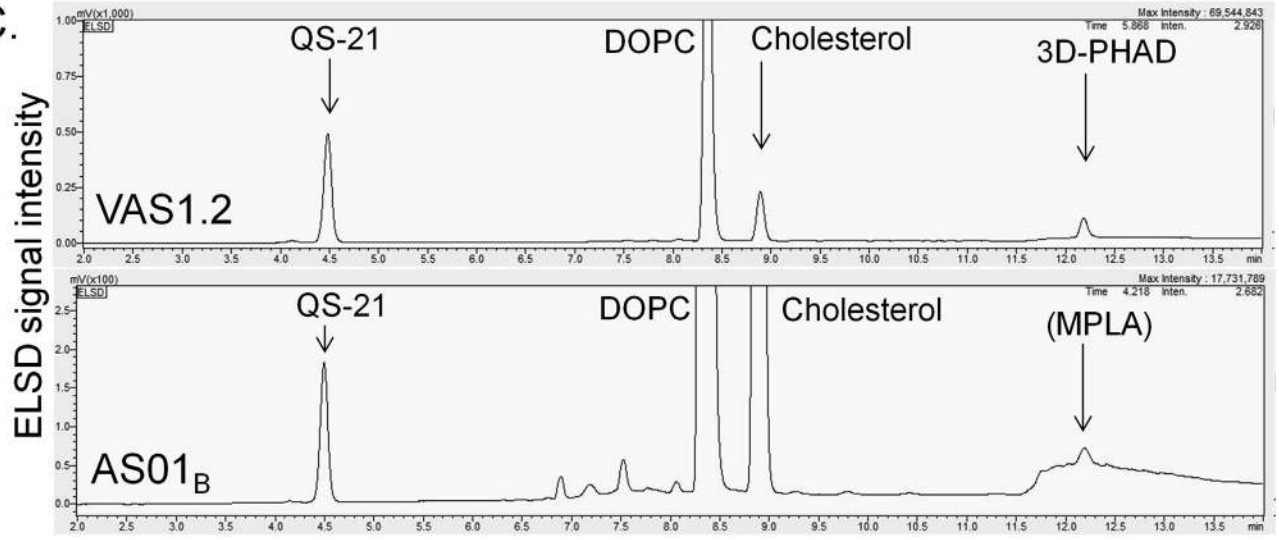

D.

	DOPC	cholesterol	% chol	QS-21	3D-PHAD	QS21:lipid
VAS1.1	**4.22**	**0.93**	18.0%	**0.50**	**N/D**	0.10
VAS1.2	**1.80**	**0.40**	18.2%	**0.50**	**0.51**	0.23
AS01$_B$	**13.44**	**4.28**	24.2%	**0.50**	**N/A**	0.03

Fig. 3. Quantitative analysis of VAS1.1, VAS1.2, and AS01$_B$. A) HPLC solvent program table for the simultaneous quantitation method with percentages listed by time phase. B) Calculated lower limits of quantitation for each of the four components detected by the method. C) Chromatograms for VAS1.2 and AS01$_B$ with identifiers for principal component peaks. D) Quantitative analysis table for VAS1.1, VAS1.2, and AS01$_B$ as assessed by the HPLC method, normalized to QS-21 content. Calculated lipid mass percentage of cholesterol is shown, as is the ratio of QS-21 to total lipid.

although geometric mean midpoint titers (GMMT) were higher with VaxiPatch delivery against all but the H3N2 strain. This indicates that reformulation and delivery of 2 μg of antigen by VaxiPatch results in equivalent responses when compared to the intramuscular control group.

By contrast, GMMT values for both adjuvanted groups (VAS1.1 and VAS1.2) were higher than for IM injection or non-adjuvanted VaxiPatch groups (p-value < 0.01 for each). The increase in titer was most evident in the case of H1N1 responses, for which VAS1.1 induced a 47-fold increase in GMMT over IM controls, and a 22-fold increase over non-adjuvanted VaxiPatches, as shown in Fig. 5A. For the AS01$_B$-like VAS1.2 adjuvant, the extent of enhancement was even greater (68-fold over IM injection and 32-fold over non-adjuvanted VaxiPatch). Comparable GMMT against the B-Victoria lineage strain (B/Colorado/06/2017) were observed in the adjuvanted groups, though the magnitude was lower by comparison (7.1 and 3.8-fold higher than IM and non-adjuvanted VaxiPatch for VAS1.1, 9.8 and 5.3-fold higher for VAS1.2 respectively; shown in Fig. 5C). Overall, IgG GMMT were lower against the H3N2 and B-Yamagata lineage components, but enhancements over IM and non-adjuvanted VaxiPatch treatments still ranged between 8.2-fold (H3N2; IM vs VAS1.2) and 19.1-fold (B-Yamagata; IM vs VAS1.2). Statistically significant differences in the GMMT were not present between the two adjuvant groups for any of the four constituent HA strains, but upward trending was notable for VAS1.2 over VAS1.1 for three of the four strains.

3.6. Functional analysis of VaxiPatch-driven immune responses

Post-vaccination sera were assessed for inhibition of hemagglutination of hRBCs by egg-derived, BPL-inactivated WHO reference standards, representing the closest-available matches to the vaccine strains. All sera were pre-treated with kaolin as described elsewhere [18]. Acquisition of a 1:40 or higher inhibition titer in the HAI test is accepted as a surrogate for seroconversion or protection in clinical studies for influenza vaccines [23].

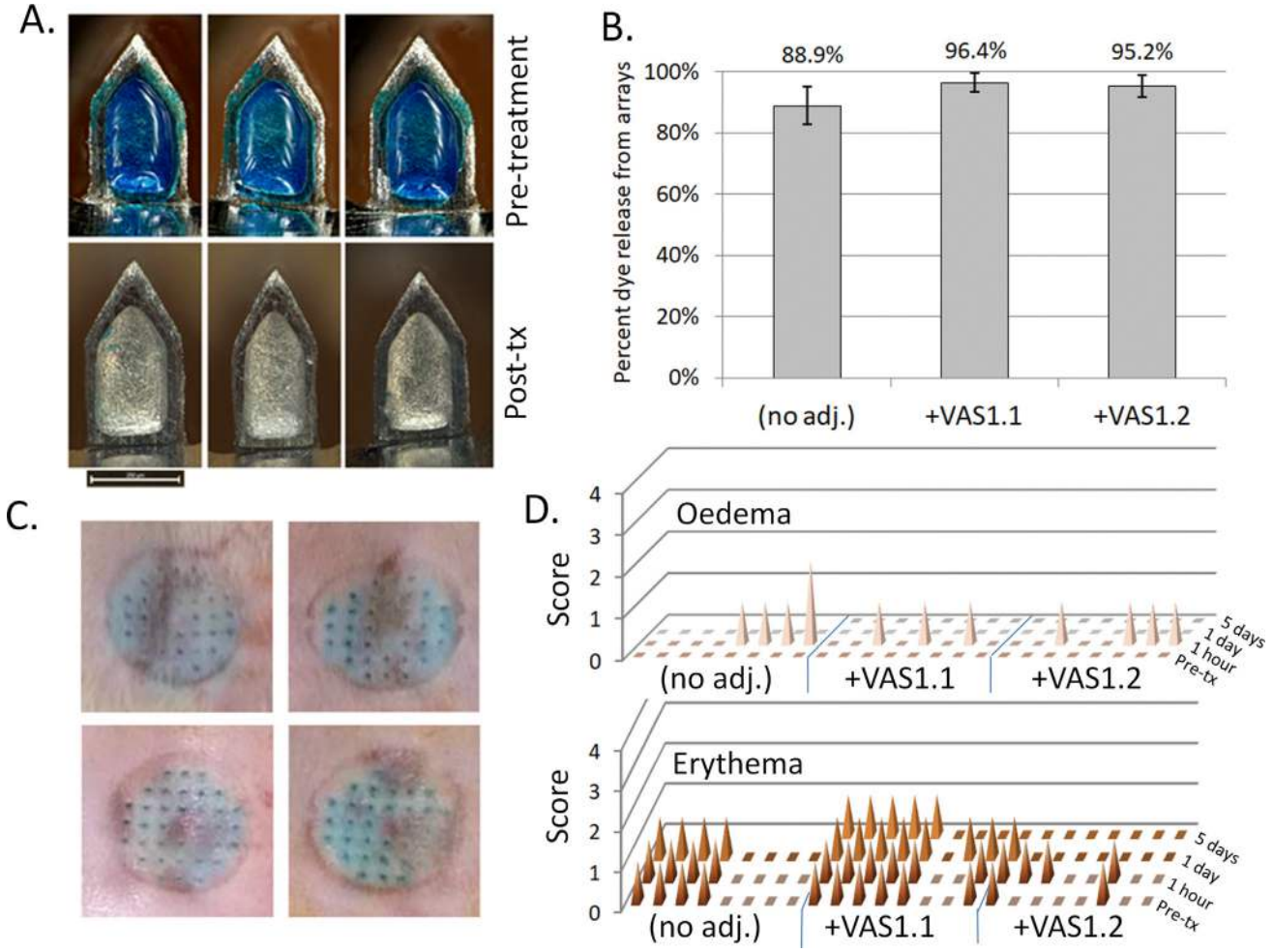

Fig. 4. VaxiPatch delivery by dye release and lack of reactogenicity *in vivo*. A) Top**.** detail images of three microarray tips, loaded with VAS1.2-adjuvanted antigen. Bottom**.** detail images of three representative tips of a VAS1.2-adjuvanted VaxiPatch after 5 min on rat skin. Scale bar shown represents 250 μm. B) Delivery estimation based on dye release (residual dye elution from spent arrays) compared to parallel control arrays. Error bars represent standard deviation (n = 8 per group). C) Four representative VaxiPatch application sites after removal of patches from the VAS1.1-adjuvanted group, showing temporary dye deposition in the pattern of the tips on the skin. D) Plot of Draize-scored (0–4) swelling and redness at the application site pre-treatment, and at 1 h, 1 day, and 5 days post-treatment. Note that day 5 evaluation was not available for the unadjuvated VaxiPatch group. Each column represents a single VaxiPatch-treated animal.

Inhibitory responses against the H1N1pdm09 strain were tested using BPL-inactivated A/Brisbane/02/2018 stock (Fig. 6A). Among the eight animals treated with the IM-injected vaccine, six gained inhibitory titers of 1:40 or above (75 % seroconversion), with a geometric mean HAI titer of 56.57. Titers observed in non-adjuvanted VaxiPatch animals were higher, with a geometric mean titer (GMT) of 61.69 (87.5 % seroconversion), though this did not reach statistical significance. All sixteen animals that received VaxiPatches with VAS1.1 or VAS1.2 responded at 1:80 or higher (100 % seroconversion) and had substantially higher GMT (P-value < 0.05 for both adjuvant groups over both non-adjuvanted groups). VAS1.1 animals had a 3-fold increase in GMT HAI over IM injected vaccine, while VAS1.2 animals were 4-fold higher.

For the H3N2 HAI responses, BPL-inactivated A/Kansas/14/2017 virus was utilized. As is shown in Fig. 6B, the vaccine was less effective against this strain, with only five of eight IM injection animals achieving titers of 1:40 or higher (62.5 % seroconversion). Non-adjuvanted VaxiPatch-delivered vaccine was less effective, with only two of eight achieving titers of 1:40 or higher (25 % seroconversion). Differences in the means of these two groups were statistically insignificant. Both VAS-adjuvanted VaxiPatch groups had higher GMT (67.27 and 56.57 respectively) and higher percent seroconversion (87.5 % for both groups) as compared to the non-adjuvanted groups. In this dataset, the only group comparison with statistical significance was the VAS1.1-adjuvanted patches over the non-adjuvanted VaxiPatch (P-value < 0.05). A small level of non-specific background was present against H3N2, with two of the IM injection animals and one of the non-adjuvanted VaxiPatch animals showing partial inhibition at 1:10 in their pre-immune sera.

The Victoria-lineage influenza B responses were tested against BPL-inactivated B/Colorado/06/2017 virus. Inhibition titers against this strain were varied, with only half of the IM-injection animals achieving 1:40 or higher titers (50 % seroconversion, GMT of 25.94), as shown in Fig. 6C. Non-adjuvanted VaxiPatches elicited better responses (62.5 % seroconversion, GMT of 30.84), but this difference was not statistically significant. When the same antigen preparation was delivered by VaxiPatch with VAS1.1, however, all eight animals seroconverted, with more than half achieving 1:80 (100 % seroconversion, GMT of 61.69). Considerable variation within group was present in the VAS1.2-adjuvanted animals, with half of the animals achieving 1:40 or higher titers and a GMT of 36.68. The large within-group variance in the B-Victoria responses precluded establishment of statistical significance for the adjuvanted groups.

The Yamagata-lineage responses were initially assessed using BPL-inactivated virus, but substantial levels of non-specific inhibi-

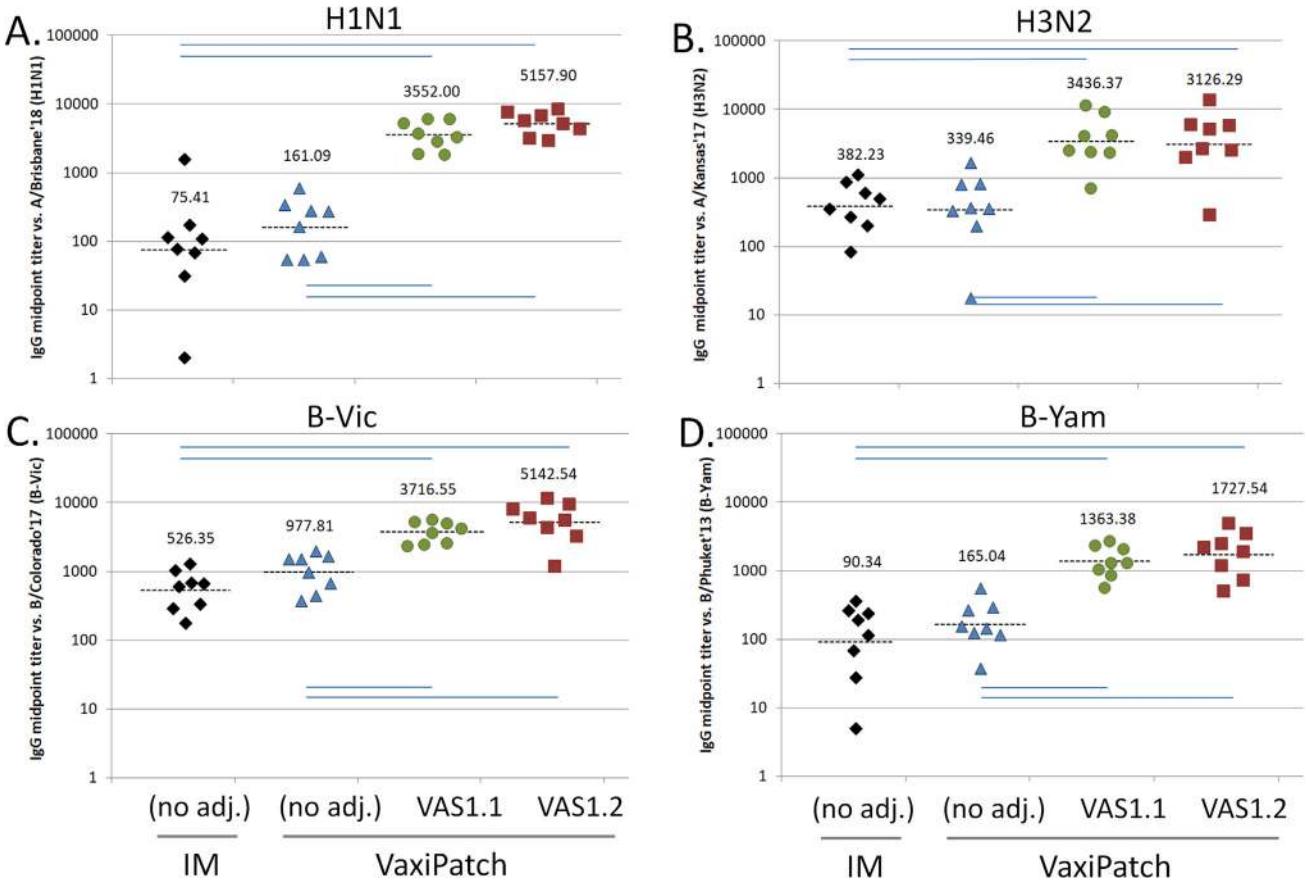

Fig. 5. Week 4 IgG ELISA titers. To provide more granular information on variation within these groups, dot plots are shown for the day 28 serum samples with recombinant HA protein representing each of the four constituent strains of the quadrivalent vaccine. A) H1N1pdm09 responses vs A/Brisbane/02/2018. B) H3N2 responses vs A/Kansas/14/2017. C) B-Victoria responses vs B/Colorado/06/2017. D) B-Yamagata responses vs B/Phuket/3073/2013. Dashed lines indicate geometric mean midpoint titers among groups. Statistical significance as determined by post-hoc Tukey's HSD tests are shown as horizontal lines between groups, each one representing significance at 0.01 or greater.

tory activity were observed in pre-immune sera. Instead, the purified B/Phuket/3073/2013 HA antigen stock from NIBSC was used for these assays. Using this reagent, a low level (1:10 inhibition) was scored for 21 of the 32 untreated animals (65.6 %), while one animal of 32 (3.125 %) inhibited at 1:20 in the pre-immune serum. HAI titers against B/Phuket/3073/2013 are plotted in Fig. 6D. Against this antigen, seroconversion was rare in the non-adjuvanted groups, with half of the IM injection animals and only two of the non-adjuvanted VaxiPatch animals achieving inhibition titers of 1:40 or above (GMT of 25.94 and 20.00, respectively). Seroconversion and geometric mean titers were higher for both adjuvanted VaxiPatch groups, with seven of eight (87.5 %) of the VAS1.1 animals achieving titers of 1:40 or above, along with six of eight (75 %) VAS1.2 animals. GMT were equal for the two adjuvanted groups, and both were significant (P-value < 0.01) over the non-adjuvanted VaxiPatch group, though not over the IM injection control. Full HAI data summary tables are included as Figure S4.

3.7. Stability of VaxiPatch-format quadrivalent influenza vaccine

To assess stability of cell-based influenza vaccine on VaxiPatch, we employed a cumulative, activity-based assay (hemagglutination), and a strain-specific serological method (SRID). Hemagglutination activity is shown in Fig. 7A. Strikingly, even arrays stored for 28 days at 60 °C retained agglutination activity by this assay. By contrast, Flucelvax exhibited a 64-fold loss of activity at 40 °C.

A more quantitative (and strain-specific) method, SRID, was also employed. Potency by strain for the 14- and 28-day time points is shown in Fig. 7B. In the case of the H1N1 strain, the potency exhibited a modest decline over the 28-day series, remaining above 58 % of initial activity even after 28 days under severe temperature stress (60 °C). H3N2 potency remained at 81.5 % or above across the series, while B-Victoria potency was at or above 78.4 % of the initial dose. The B-Yamagata lineage component remained>73 % active at 28 days.

Cumulatively, these data demonstrate that the VaxiPatch format confers a high level of thermostability, based both on a functional assay (hemagglutination) and an industry-standard serological method (SRID).

4. Discussion

This work describes the use of Flucelvax and the adjuvants VAS1.1 and VAS1.2 delivered on a skin patch, VaxiPatch. SRID analysis indicated that potent HA material was retained across reformulation for all four strains under the conditions employed. The hemagglutination assay served as an effective rapid screen for cumulative overall activity for process development. Similarly, we used an overall protein concentration, as assessed by BCA assay, to guide antigen loading of VaxiPatch arrays. We calculate that the 2 μg total protein dose printed to arrays included between 0.44 and 0.6 μg of potent HA per strain.

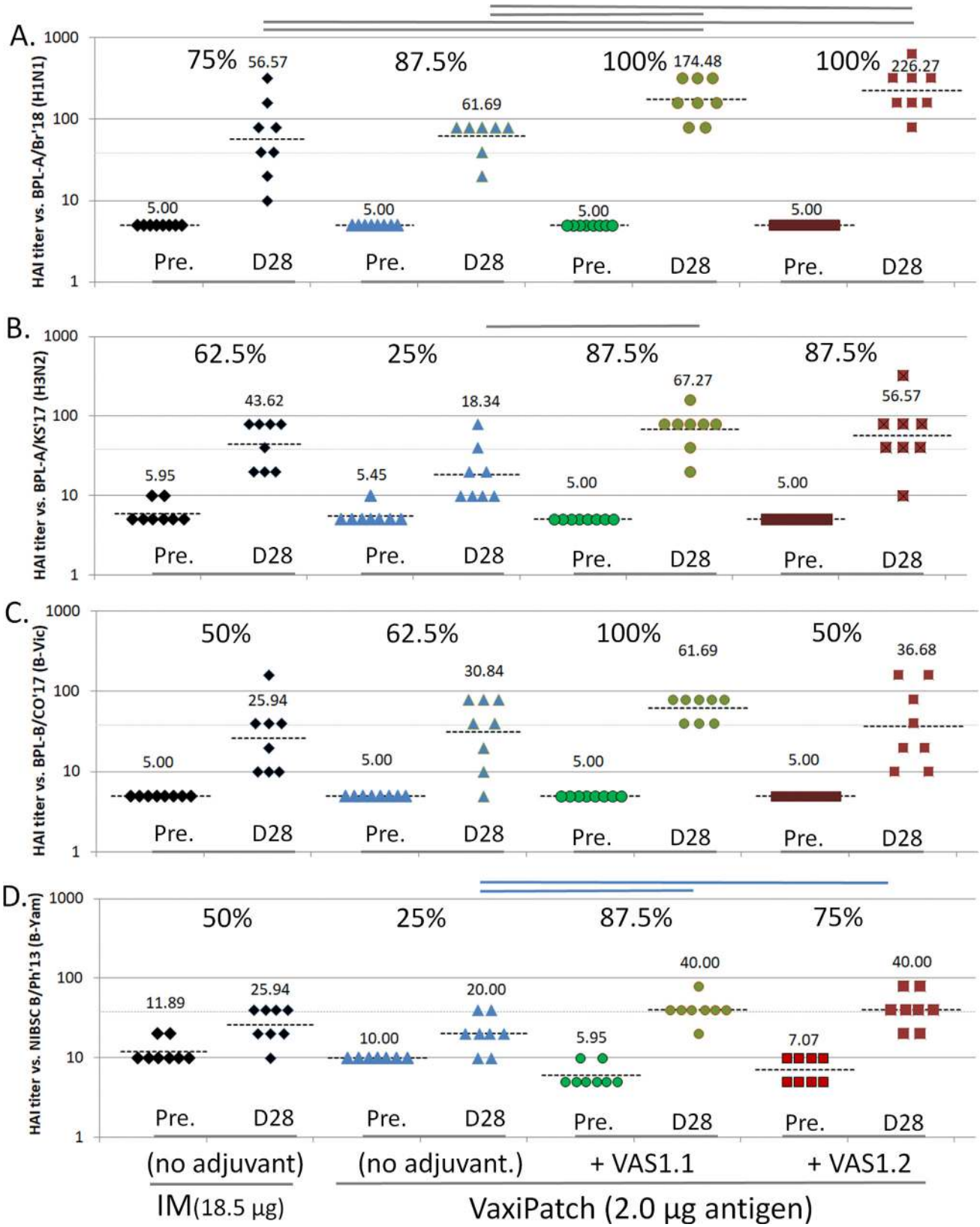

Fig. 6. Hemagglutination Inhibition Titers at Week 4. Rat serum was tested for its ability to inhibit the agglutination activity of cognate reference antigens, before and 28 days after vaccination. Dashed lines represent geometric mean HAI titers within each group. Statistical significance is indicated above plots where present, based on post-hoc Tukey's HSD tests. Blue lines connect groups with <0.01 significance, while gray lines connect those groups with significant differences at a 0.05 threshold. Horizontal gray dotted line on each plot graphically represents 1:40 threshold for seroconversion. Percent seroconversion (% animals gaining 1:40 or higher titers) are shown above each dataset, between pre- and post-treatment results. Treatment groups are defined at the bottom of the figure: black diamonds for IM controls, blue triangles for VaxiPatch without adjuvant, green circles for VaxiPatch +VAS1.1, and red squares for VaxiPatch +VAS1.2. A) H1N1pdm09-specific responses against BPL-A/Brisbane/02/2018. B) H3N2-specific responses against BPL-A/Kansas/14/2017. C) B-Victoria-specific responses against BPL-B/Colorado/06/2017. D) B-Yamagata-specific responses against NIBSC purified B/Phuket/3073/2013 HA antigen.

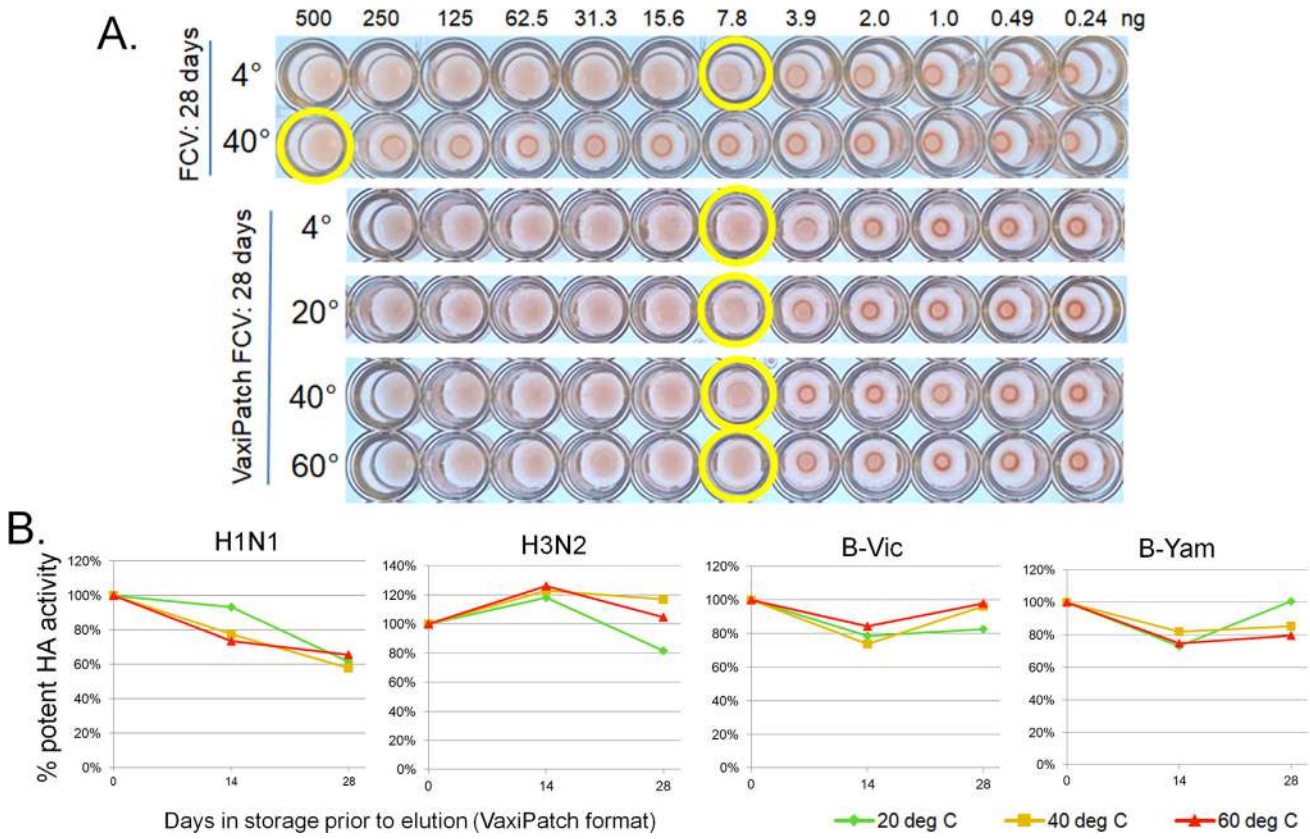

Fig. 7. Stability of VaxiPatch-format Quadrivalent Influenza Vaccine. A) Hemagglutination assay performed on liquid Flucelvax stored at 4 or 40 °C for 28 days, as compared to the same material eluted from VaxiPatch arrays after 28 days of storage at 4, 20, 40, or 60 °C. B) Time course of potent HA dose per strain on non-adjuvanted VaxiPatches printed with 4 μg of Flucelvax and stored in foil pouches with desiccant at 20, 40, or 60 °C for 28 days, based on SRID of eluted material.

We used thin-film hydration and extrusion as a manufacturing process for our liposomal adjuvants VAS1.1 and VAS1.2. We developed methods to quantitatively measure all adjuvant components and enable comparison of VAS1.2 and $AS01_B$. VAS1.2 and $AS01_B$ particles were indistinguishable by CryoEM and DLS. The higher adjuvant content per liposome of VAS1.2 gave a zeta potential of −48.2 mV versus −29.5 mV for $AS01_B$.

The $AS01_B$ component of an IM Shingrix dose is 50 μg each of QS-21 and MPLA, 100 times higher than the 0.5 μg loaded onto each VaxiPatch. This same fractional adjuvant dose has been proposed for use in clinical studies of VaxiPatch. We saw little to no evidence of skin reactogenicity in the rats receiving adjuvanted VaxiPatches. Light erythema (score = 1) was frequently scored by veterinary technicians *prior to* VaxiPatch application and described to be associated with the periphery of the zone of depilation. Swelling, when present, fully resolved after 1 h. No increase in swelling was observed for adjuvanted VaxiPatches. High levels of delivery (89 % and above) were consistently achieved using 5-minute treatments. Analysis of antigen-specific midpoint IgG titers by ELISA provided evidence of non-inferiority using VaxiPatch compared to intramuscular injection. We did not examine dose-response for the intramuscular Flucelvax control in rats, so we cannot determine whether the 18.5 μg dose used here was saturating, or make specific inferences regarding dose sparing of the non-adjuvanted product when delivered intradermally. When VAS1.1 or VAS1.2 was co-formulated on VaxiPatch with 2 μg of Flucelvax, antigen-specific IgG titers markedly increased as compared to 50 μL of the vaccine delivered IM. HAI GMTs for the H1N1 strain significantly increased with VAS1.1 and VAS1.2 over non-adjuvanted groups. Overall HAI improvements against the other three strains from adjuvanted VaxiPatches were modest compared to IgG midpoint titer enhancements. This could stem from subtle differences between the cell-based strains of Flucelvax, and the egg-derived reference antigens used for the HAI assay, or from the age of the vaccine material (made available for use 10 months post-expiry). Still, higher seroconversion rates were observed across three of the four strains for VAS1.2, and all four for VAS1.1.

The preliminary stability studies presented here suggest that reformatting Flucelvax onto VaxiPatch confers a high level of thermostability, even under substantial heat stress (60 °C for 28 days). The retention of potency by SRID was further supported by functional analysis using the hemagglutination assay. This level of thermostability could be transformative in the context of a pandemic or biodefense response, or for applications where the cold chain remains limiting.

In summation, use of VAS1.1 or VAS1.2 adjuvants in combination with VaxiPatch yielded dramatically increased antigen-specific antibody titers (7–47 fold or 8–68-fold higher, respectively), as well as providing increases in seroconversion. Future studies may explain why these increases were not associated with statistically significant increases in functional HAI titers. The levels of QS-21 and 3D-PHAD loaded per dose were 100-fold less than the clinical dose of the analogous $AS01_B$ adjuvant in Shingrix. Cumulatively, the combination of a 2 μg antigen dose, ease of administration, lack of reactogenicity, and thermostability could be transformative for a vaccine application with a global market.

Data availability

Data will be made available on request.

Declaration of Competing Interest

The authors declare the following financial interests/personal relationships which may be considered as potential competing interests: Daniel Henderson reports financial support was provided by Verndari Inc. Daniel Henderson reports a relationship with Verndari Inc that includes: board membership, employment, and equity or stocks. Daniel Henderson has patent #US Patent 10,022,436 "Microneedle compositions and methods of using same" issued to Verndari Inc. Daniel Henderson is a founder and former CEO of Verndari Inc. He currently holds stock and received salary from Verndari during the conduct of this study.

All authors are employees of Verndari, Inc, hold stock options, and are listed as inventors on U.S. Patent Applications assigned to Verndari.

Acknowledgments

We thank the UC Davis Venture Catalyst Program of which Verndari is a member. We thank Delena Gamez for her assistance in the conduct of this study.

Funding sources

The majority of this work was funded by Verndari Inc. Development of analytical methods for the VAS1.2 adjuvant was partially funded by BARDA DRIVe contract EZ-BAA - 75A50120C00153, for further development of Verndari's alternative vaccine delivery platform.

Author contributions

TE designed and performed most of the lab work. GT and TE printed the microarray patches and GT performed many of the assays. DH conceived this work, designed and oversaw VaxiPatch fabrication, and directed the lab. TE and DH wrote the manuscript.

Appendix A. Supplementary data

Supplementary data to this article can be found online at https://doi.org/10.1016/j.vaccine.2022.10.006.

References

[1] Milián E, Kamen AA. Current and emerging cell culture manufacturing technologies for influenza vaccines. Biomed Res Int 2015;2015():504831.
[2] Sparrow E, Wood JG, Chadwick C, Newall AT, Torvaldsen S, Moen A, et al. Global production capacity of seasonal and pandemic influenza vaccines in 2019. Vaccine 2021;39(3):512–20.
[3] Weir JP, Gruber MF. An overview of the regulation of influenza vaccines in the United States. Influenza Other Respir Viruses 2016;10(5):354–60.
[4] Chung JR, Kim SS, Kondor RJ, Smith C, Budd AP, Tartof SY, et al. Interim Estimates of 2021–22 Seasonal Influenza Vaccine Effectiveness - United States, February 2022. MMWR Morb Mortal Wkly Rep 2022;71(10):365–70.
[5] Polack FP, Thomas SJ, Kitchin N, Absalon J, Gurtman A, Lockhart S, et al. Safety and Efficacy of the BNT162b2 mRNA Covid-19 Vaccine. N Engl J Med 2020;383 (27):2603–15.
[6] Baden LR, El Sahly HM, Essink B, Kotloff K, Frey S, Novak R, et al. Efficacy and Safety of the mRNA-1273 SARS-CoV-2 Vaccine. N Engl J Med 2021;384 (5):403–16.
[7] Dormitzer PR. Rapid production of synthetic influenza vaccines. Curr Top Microbiol Immunol 2015;386:237–73.
[8] Chivukula S, Plitnik T, Tibbitts T, Karve S, Dias A, Zhang D, et al. Development of multivalent mRNA vaccine candidates for seasonal or pandemic influenza. npj Vaccines 2021;6(1).
[9] Dolgin E. mRNA flu shots move into trials. Nat Rev Drug Discov 2021;20 (11):801–3.
[10] Cohen DA et al. Are COVID-19 mRNA vaccine side effects severe enough to cause missed work? Cross-sectional study of health care-associated workers. Medicine 2022;101(7):. https://doi.org/10.1097/MD.0000000000028839e28839.
[11] Montano D. Frequency and Associations of Adverse Reactions of COVID-19 Vaccines Reported to Pharmacovigilance Systems in the European Union and the United States. Front Public Health 2021;9:756633.
[12] Sun J, Zhang M, Gehl A, Fricke B, Nawaz K, Gluesenkamp K, et al. Dataset of ultralow temperature refrigeration for COVID 19 vaccine distribution solution. Sci Data 2022;9(1). https://doi.org/10.1038/s41597-022-01167-y.
[13] Brockman MA et al. Reduced Magnitude and Durability of Humoral Immune Responses to COVID-19 mRNA Vaccines Among Older Adults. J Infect Dis 2022;225(7):1129–40.
[14] Li APY, Cohen CA, Leung NHL, Fang VJ, Gangappa S, Sambhara S, et al. Immunogenicity of standard, high-dose, MF59-adjuvanted, and recombinant-HA seasonal influenza vaccination in older adults. npj Vaccines 2021;6(1).
[15] Li Z, Zhao Y, Li Y, Chen X. Adjuvantation of Influenza Vaccines to Induce Cross-Protective Immunity. Vaccines (Basel) 2021;9(2):75.
[16] Okayasu H, Sein C, Chang Blanc D, Gonzalez AR, Zehrung D, Jarrahian C, et al. Intradermal Administration of Fractional Doses of Inactivated Poliovirus Vaccine: A Dose-Sparing Option for Polio Immunization. J Infect Dis 2017;216(suppl_1):S161–7.
[17] Pilkington V, Keestra SM, Hill A. Global COVID-19 Vaccine Inequity: Failures in the First Year of Distribution and Potential Solutions for the Future. Front Public Health 2022;10:821117.
[18] Ellison TJ, Talbott GC, Henderson DR. VaxiPatch™, a novel vaccination system comprised of subunit antigens, adjuvants and microneedle skin delivery: An application to influenza B/Colorado/06/2017. Vaccine 2020;38(43):6839–48.
[19] Burny W et al. Different Adjuvants Induce Common Innate Pathways That Are Associated with Enhanced Adaptive Responses against a Model Antigen in Humans. Front Immunol 2017;8:943.
[20] Coccia M et al. Cellular and molecular synergy in AS01-adjuvanted vaccines results in an early IFNγ response promoting vaccine immunogenicity. npj Vaccines 2017;2:25.
[21] Didierlaurent AM, Laupèze B, Di Pasquale A, Hergli N, Collignon C, Garçon N. Adjuvant system AS01: helping to overcome the challenges of modern vaccines. Expert Rev Vaccines 2017;16(1):55–63.
[22] Izurieta HS, Wu X, Forshee R, Lu Y, Sung H-M, Agger PE, et al. Recombinant Zoster Vaccine (Shingrix): Real-World Effectiveness in the First 2 Years Post-Licensure. Clin Infect Dis 2021;73(6):941–8.
[23] Wei C-J, Crank MC, Shiver J, Graham BS, Mascola JR, Nabel GJ. Next-generation influenza vaccines: opportunities and challenges. Nat Rev Drug Discov 2020;19(4):239–52.